Understanding the Interface of Liquids with an Organic Crystal Surface from Atomistic Simulations and AFM Experiments
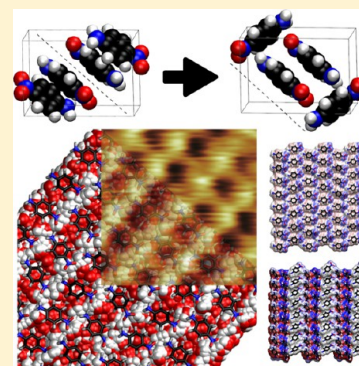
Peter Spijker,*[,†] Takumi Hiasa,[‡] Tiziana Musso,[†] Rina Nishioka,[‡] Hiroshi Onishi,[‡] and Adam S. Foster[†]

[†]COMP, Department of Applied Physics, Aalto University, Otakaari 1, FI-00076 Helsinki, Finland
[‡]Department of Chemistry, Kobe University, 1-1 Rokkodai, Kobe 657-8501, Japan

ABSTRACT: A strong ordering of solvent molecules in the solid−liquid interface of a typical and characteristic organic crystal (*p*-nitroaniline) is observed in state-of-the-art atomic force microscopy experiments. In the current work, we use both molecular dynamics (MD) simulations and experiments in different solvents to provide a detailed understanding of the nature of the solid−liquid interface. The strong ordering of solvent molecules at the surface of *p*-nitroaniline is confirmed in general, but the MD simulations point to several different possible surface reconstructions, offering different ordering of water on the surface. The calculated water density profiles and local surface hydration energies suggest a novel surface structure, which is in excellent agreement with the majority of experimental results and stands as a challenge for future diffraction techniques. Our joined theoretical and experimental study emphasizes the power of high-resolution techniques to probe the solid−liquid interface in 3D while demonstrating the importance of including systematic simulation approaches to confirm the details of the molecular structure and to increase our understanding of complex heterogeneous solid−liquid interfaces.

■ INTRODUCTION

In many nanoscale applications, the interface between the solid and the solvent is of crucial importance. These solid−liquid interfaces play, for instance, a fundamental role in electrochemistry,[1] self-assembly,[2] or biomolecular functions.[3] The precise interactions between the solid and the liquid determine many of the properties of such interfaces, including the arrangement of the liquid molecules at the surface of the solid. This arrangement is even more enhanced based on the functional groups of the solid exposed at the surface, which are, in the case of water as a solvent, often categorized in hydrophilic or hydrophobic groups.

Traditionally, diffraction techniques are used to investigate the structure of the solid−liquid interface, but these techniques are typically limited to regular and homogeneous surfaces.[4] Atomic force microscopy (AFM) overcomes this limitation and is able to visualize the topography of surfaces and interfaces at a molecular level[5] all the way down to atomic resolutions,[6,7] either under vacuum conditions or immersed in a liquid.[8,9] Recently it has been demonstrated that when operating in a dynamic mode (oscillating near the surface), the AFM is also capable of providing atomic-scale details about the structure of the final liquid layers between the AFM tip and the solid surface.[10] It has even been possible to construct full 3-D force maps of an AFM tip scanning the surface in liquid, providing unprecedented information on the hydration layers on the surface.[9,11−13] However, a quantitative link between the real hydration layers of the surface and their convolution with the AFM imaging mechanism and the tip's hydration layers remains a significant challenge.

To investigate the effect of hydrophilic and hydrophobic surface groups on the structuring of the interfacial liquid, we recently performed AFM experiments on the *p*-nitroaniline−water interface.[14] We used the organic compound *p*-nitroaniline ($H_2NC_6H_4NO_2$) as an example because the molecule contains two polar groups (amino and nitro) present on opposite ends of a nonpolar benzene ring (phenylene), allowing the control of the heterogeneity of the surface. Understanding how the interfacial water structures itself near this organic compound is an important benchmark case, which allows us to better understand dissolution and crystallization processes. In medical applications, *p*-nitroaniline is often used as a model to study the crystallization of medical compounds, which is an important issue in the pharmaceutical industry as controlling the solubility is key in the development of medicines.[15]

The bulk crystal structure of *p*-nitroaniline was investigated in detail up to the early 1960s[16−18] and again in the 1990s.[19,20] These studies showed *p*-nitroaniline to be a monoclinic (almost orthorhombic) crystal belonging to the $P2_1/m$ space group, where the preferred cleavage plane is supposedly along the (101) plane, which also provides a well-developed facet for recrystallization.[16] The unit cell (containing four *p*-nitroaniline molecules) along with an impression of the (101) plane is shown in Figure 1a,b. The plane of the *p*-nitroaniline molecule is aligned with the preferred cleavage plane, with both the hydrophilic end groups and the hydrophobic core exposed to

(a) $P2_1/m$ unit cell

(b) $P2_1/m$ (101) top view

(c) $P2_1/c$ unit cell (see text)
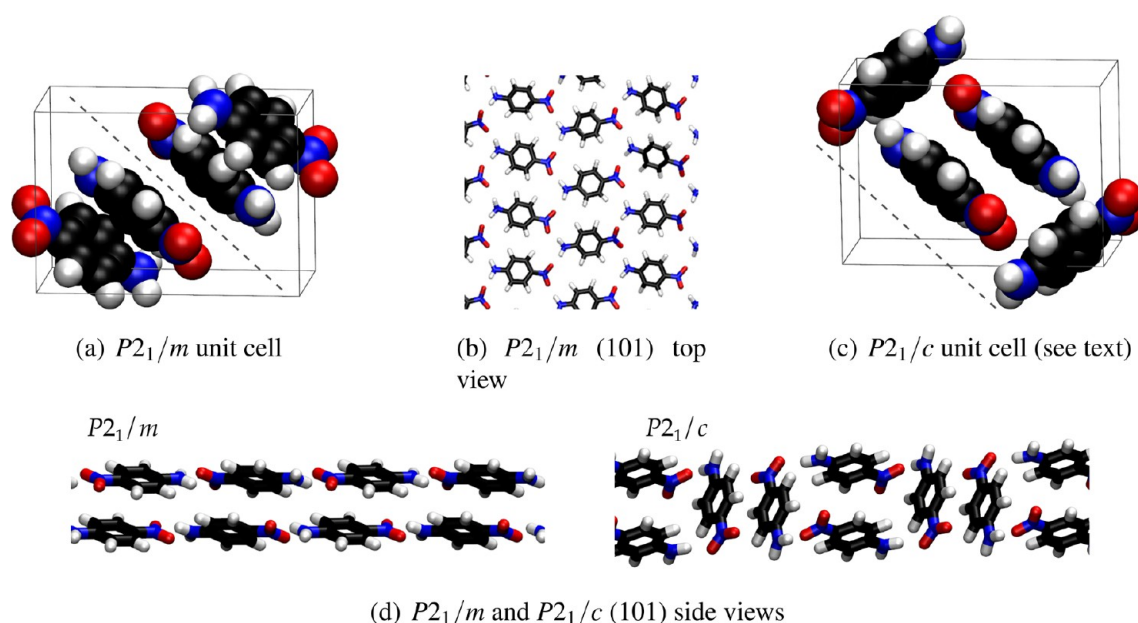
(d) $P2_1/m$ and $P2_1/c$ (101) side views

Figure 1. (a) Unit cell of *p*-nitroaniline according to the $P2_1/m$ space group is shown. The solid lines denote the borders of the unit cell, and the dashed line indicates the preferred (101) cleavage plane, which can be seen in panel b. The unit cell for the different space group representation $P2_1/c$ (see the text for Discussion) is shown in panel c, again with the (101) cleavage plane indicated by the dashed line. (d) Side views of the (101) surfaces (which is perpendicular to the page) for $P2_1/m$ and $P2_1/c$. For $P2_1/m$, two layers are visualized, whereas for $P2_1/c$ only one "layer" is shown. (See the text for more discussion on the layer definition.) In all images, black atoms denote carbon, red atoms denote oxygen, blue atoms denote nitrogen, and white atoms denote hydrogen.

the liquid. As such, a different hydration structure is expected to arise over these different groups.

In previous studies,[14] our frequency-modulated AFM experiments were able to determine the cross-sectional distributions of the force applied to the tip, and we attempted to relate these to the local density of the water structured near the interface. We noted force modulations at specific spots on the surface, which suggests water localization on the polar groups, and this was supported by preliminary force simulations. However, these simulations were relatively simple and ignored many features (such as the presence of water and the dynamics of the system) that can have a profound influence on the AFM measurement.[21,22] To rectify this and provide a more comprehensive model, in this work, we revisit the experimental results on *p*-nitroaniline in water we previously obtained and also extend them with AFM measurements of *p*-nitroaniline immersed in 1-octanol (hereafter referred to as octanol). This time we also model the solid–liquid interface between *p*-nitroaniline and both solvents using large-scale molecular dynamics (MD) simulations. Our simulations shed new light on the possible hydration structures forming at the interface and also on the surface layer structure of *p*-nitroaniline itself. In the next section, we briefly discuss the used methods and their verification and validation.

■ METHODS

On the basis of some of the earliest crystallographic work on *p*-nitroaniline, we obtained the coordinates of the non-hydrogen (heavy) atoms of a single molecule within the unit cell.[18] The lacking hydrogens were placed manually into the system by obeying the known distances and angles between the heavy atoms and the hydrogens and by knowing the hydrogens must remain in the same molecular plane as all heavy atoms. By

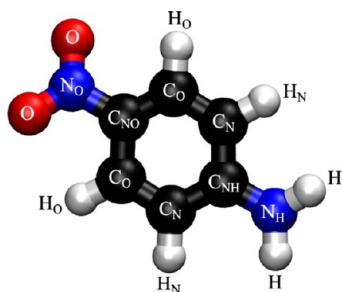further using *p*-nitroaniline's space group definition, we constructed a complete unit cell.

Because of the organic nature of *p*-nitroaniline and its solvation in either water or octanol, we decided to use the well-established empirical biological force field CHARMM for all of our MD computations.[23] However, crystallization is rarely the aim of biological atomistic force fields and CHARMM might be an ill-suited choice for the solid phase of *p*-nitroaniline. Because the most important element determining the crystallization is the electrostatic interaction between the molecules,[24] we decided to optimize the charge distribution on the *p*-nitroaniline molecules but to leave all other parameters untouched, as to not disturb the carefully balanced van der Waals interactions between solvent and solutes in the CHARMM force field.

To optimize these electrostatic interactions, we used first-principles computations employing a spin-polarized density functional theory (DFT) with a plane-wave basis-set, as implemented in the VASP package[25,26] using the Perdew–Burke–Ernzerhof exchange-correlation functional.[27] Noncovalent interactions are described by means of the most recent version of the Langreth–Lundqvist density functional vdW-DF2,[28] and the nonlocal term in it was evaluated using the adaptive real-space approach.[29] The core electrons are described by using projected augmented wave (PAW) potentials.[30,31] For *p*-nitroaniline, the potentials are generated in the following electron configurations: H ($1s^1$), C ($[1s^2]$-$2s^22p^2$), N ($[1s^2]2s^22p^3$), and O ($[1s^2]2s^22p^4$) with the core electrons given in square brackets. The energy and *k*-point convergence were checked carefully, and the geometry of the bulk unit cell was checked relaxing the cell shape at a variety of constant volumes. The optimized charges were computed on the charge density provided from the DFT computation using the grid-based Bader analysis algorithm. The atomic charges are

obtained from an algorithm that partitions the charge-density grid into Bader volumes.[32]

After a careful optimization using the DFT/Bader approach, we used the obtained charges and crystal structure to build a larger ($4 \times 4 \times 4$ unit cells, 256 molecules) bulk crystal and then used MD to allow this crystal to equilibrate from 0 to 300 K at ambient pressure. All MD simulations are performed using the MD code NAMD.[33] From the obtained crystal structure, a unit cell is extracted and used for another DFT/Bader computation. This process has been repeated several times until convergence is achieved to a high accuracy of both the charges and the shape of the unit cell. The optimized unit cell was found to be slightly shorter along the a axis and slightly larger along the c axis, with the b axis almost unchanged. Recent work on p-nitroaniline derivatives also shows slight changes in crystal structure with respect to previous experiments,[34] supporting our first-principles computations. In Table 1, the

Table 1. Original CHARMM Charges (in units of electric charge e) and Charges after DFT/Bader/MD Optimization for p-Nitroaniline[a]

atom	CHARMM	optimized	difference
C_N	−0.180	0.020	0.200
H_N	0.160	0.110	−0.050
C_O	−0.115	0.022	0.137
H_O	0.115	0.055	−0.060
C_{NH}	0.050	0.490	0.440
N_H	−0.850	−1.289	−0.439
H	0.400	0.495	0.095
C_{NO}	0.320	0.250	−0.070
N_O	0.400	0.205	−0.195
O	−0.340	−0.530	−0.190

[a]Naming convention for each of the atoms is depicted in the image above the Table.

original charges (according to the CHARMM force field) and the final ones obtained from our iterative charge optimization are given, showing the most significant change being a stronger dipole occurring on the amino-phenyl coupling (by as much as 0.88 e).

We used these optimized p-nitroaniline unit cells to construct a larger bulk crystal (576 p-nitroaniline molecules, approximately $4.5 \times 5.3 \times 3.5$ nm), which we rotated to align the (101) plane with the xy plane of the simulation box. Because p-nitroaniline molecules lie entirely within this plane, we count a total of 12 parallel layers in our crystal. To ensure its stability, we performed 50 ps MD simulations for both a bulk system and a system with the (101) surface exposed to vacuum (free surface). Both systems showed high stability, which strengthens our assumptions on the iterative scheme to optimize the charges on the p-nitroaniline molecule. Also, the periodic structure appearing on the surface (the observed unit cell)

measured 0.60×1.47 nm, which is very close to the one obtained from our experiments ($\sim 0.6 \times 1.5$ nm).[14]

The system with the free surface is subsequently solvated with water on the outside of both (101) surfaces of the crystal, where the center of the crystal was placed in the center of the simulation box to facilitate easier analysis after the simulations. As periodic boundaries are applied in all directions, we have to ensure that the water part is thick enough in the direction perpendicular to the surface (in our case, the z direction) so that the periodic images do not interfere with each other and also that it extends sufficiently far away from the surface to achieve bulk properties again. The fully water solvated system measures approximately $4.5 \times 5.3 \times 13.0$ nm and contains ~ 30 000 atoms (576 p-nitroaniline and 6924 water molecules).

Initially, the system's energy is minimized for several steps (2500 steps while all p-nitroaniline molecules are kept fixed and 500 steps with all water molecules fixed), followed by a short (10 ps, 1 fs time step) equilibration under ambient conditions (1 atm, 310 K). This process allows the system to be in its energetic minimum configuration. A longer MD simulation of 250 ps, under constant ambient conditions, is used to collect data.

For visual inspection, VMD was used,[35] and most of the analysis was performed using the Python library MDAnalysis.[36] This current simulation setup and protocol is similar to the setup used previously to study the interaction between water, ions, and calcite or muscovite.[12] We deliberately ignore the AFM tip in all our MD simulations, using an equilibrium approximation, as we wish to focus on the hydration structures arising at the p-nitroaniline solid−liquid interface and the structure of the surface itself rather than on the details of the convolution with the tip's solvation layers.[21,37] Furthermore, because the oscillation frequency is orders of magnitude smaller than the molecular motion of the water, we feel it is also a reasonable approximation to ignore any hydrodynamic effects within the simulations.

Space Group Representations. In the previous papers on p-nitroaniline the space group to which this crystal belongs was identified as being $P2_1/n - C_{2h}^5$, which is a nonstandard setting of the space group $P2_1/c$,[38] but judging from the images provided in these previous papers it is more likely that the space group $P2_1/m$ is meant. To account for this ambiguity, we repeated the entire initialization of the simulation setup with the $P2_1/c$ space group setting as well. In Figure 1c, the unit cell for this representation is shown.

The DFT/Bader/MD charge optimization for the $P2_1/c$ representation did not show any great difference with the one obtained from the other representation, which is another strong argument for the accuracy of the used first-principle methods. The unit cell for $P2_1/c$ differs considerably from the original one, but the observed unit cell on the (101) surface is remarkably similar to the one for the $P2_1/m$ representation (0.55×1.52 nm for $P2_1/c$, 0.60×1.47 nm for $P2_1/m$), which lies within the experimental accuracy for determining the size of the observed unit cell. Because of the change in the shape of the unit cell, the size of the crystal used in the MD simulations is also different. Instead of the 12 layers with the p-nitroaniline molecules, this crystal is build up by eight thicker layers. In each of the thicker layers, two p-nitroaniline molecules are parallel to the plane, whereas two other molecules are perpendicular. The width of the plane is thus about similar to the length of the p-nitroaniline molecule. In Figure 1d, for both space-group representations, a side view of one or two layers is shown. So,
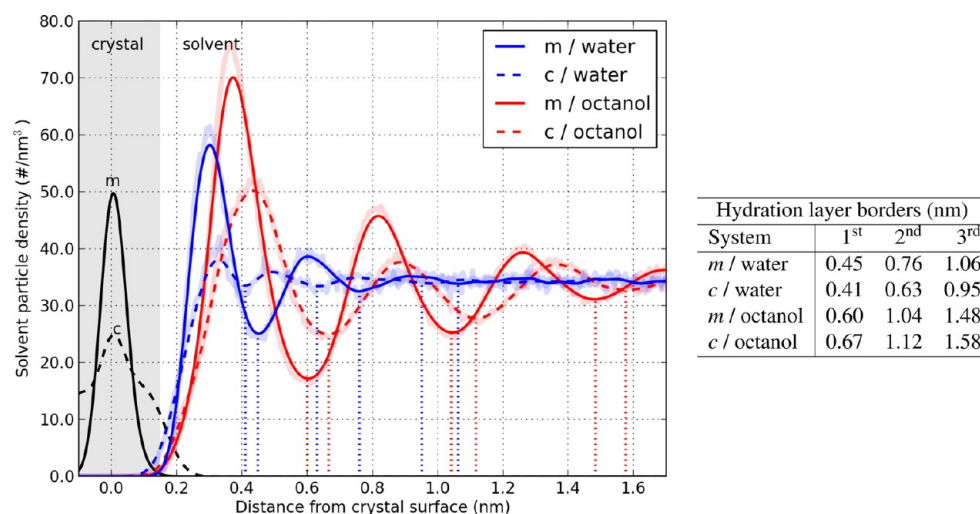
Figure 2. Time-averaged particle density (in number of particles per cubic nanometer) of the solvents is shown for all simulations as a function of the distance to the crystal surface. The distances are measured with respect to the center of the in-plane molecules in the outermost layer of the crystal, which is set at zero (black lines to the left indicate the crystal densities, not to scale). Water is depicted in blue, octanol is depicted in red; the *m*-crystal data are drawn in solid lines, and the *c*-crystal data are drawn in dashed lines. All lines are slightly smoothed to enhance their presentation, but for the solvents, the actual data are shown in the graph as faint lines in the background. The vertical dotted lines dropping down to zero indicate the location of the minima in each of the density plots, which are the borders of the hydration layers. (The values are in the table to the right.)
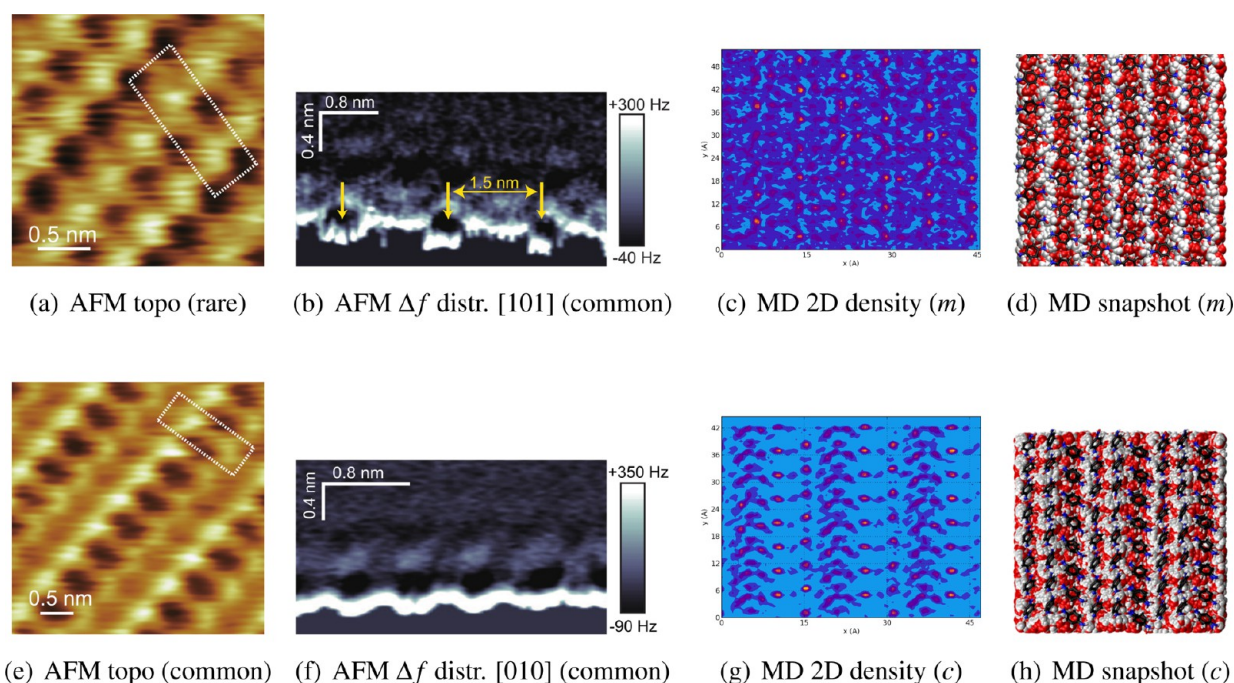

Figure 3. In panels a, b, e, and f, the experimental results from ref 14 are shown. The two cross-sectional Δf distributions (b,f) are both for the topography depicted in panel e. In panels c and g, the 2D particle density distributions obtained from the MD simulations for the first hydration layer parallel to the surface are shown for the *m*-crystal and *c*-crystal, respectively. In panels d and h, time-accumulated MD snapshots of the water molecules on the (101) surface are shown. The underlying structure of the crystal lattice is also shown.

one $P2_1/c$ layer is as thick as two $P2_1/m$ layers. Consequently, the $P2_1/c$ version of the system contains a different amount of molecules (768 *p*-nitroaniline molecules and 8810 water molecules), but the same care has been taken with the addition of water to solvate the systems, so all prerequisites are met.

In the remainder of the paper, both systems will be compared with each other (in their energetics and stability), and both of them will be compared with the experimental results. For simplicity, we will refer to both systems as the *m*-crystal and *c*-crystal, respectively, the $P2_1/m$ and $P2_1/c$ space group settings of the crystal.

Octanol. In our previous work,[14] we only reported AFM experiments on *p*-nitroaniline with water as the solvent. Since then we have also conducted AFM experiments where water has been exchanged by octanol. For the experimental part the exact same setup as explained in our previous work has been used. Here we report the topography results of those experiments along with the results for the MD simulations; see Figure 5.
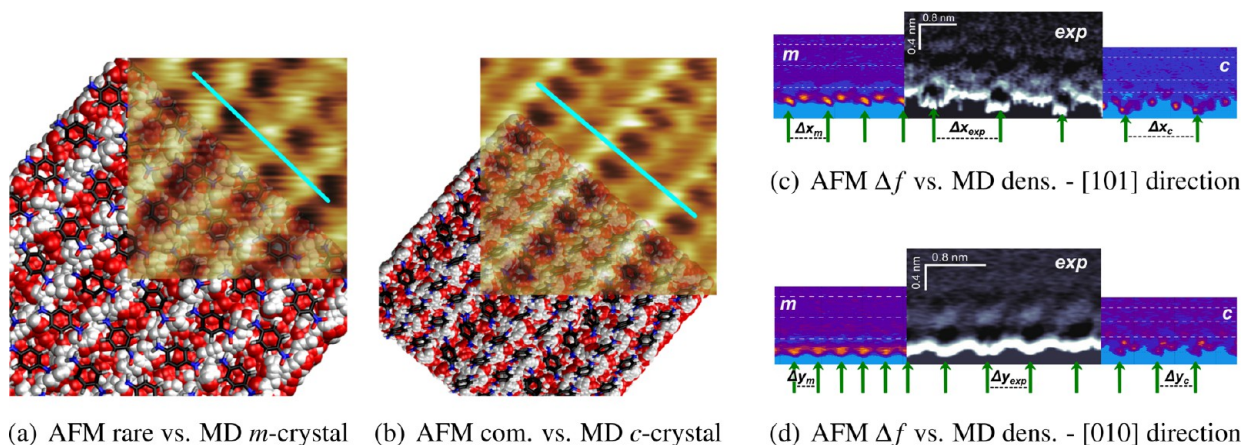
(a) AFM rare vs. MD *m*-crystal (b) AFM com. vs. MD *c*-crystal

(c) AFM Δf vs. MD dens. - [101] direction

(d) AFM Δf vs. MD dens. - [010] direction

Figure 4. Composite images of AFM experiments and MD simulations. In panels a and b, topographic images from the rare and common AFM experiments are compared with the MD snapshots for the *m*-crystal and *c*-crystal, respectively. In panels c and d, the experimental Δf distributions from the common case (in both the [101] and [010] direction) are compared with the cross-sectional density plots from the MD simulations for both crystal arrangements (indicated by an *m* or a *c*). The green arrows point to similar features appearing in each image, with the corresponding spacing indicated as well. Both lines in panels a and b indicate along which line the experimental cross sections have been taken.

Because octanol is a much larger molecule than water, its self-diffusivity is much lower. Where a MD simulation of 250 ps with water is long enough to obtain reliable statistics, much longer runs are required in the case of octanol. Therefore, we extended our runs to cover 3 ns (using the same 1 fs time step). Another disadvantage is that octanol can be adsorbed onto the *p*-nitroaniline surface in its entire length, and with the small surface area used for the water simulations, the risk of influence across the periodic boundaries is present. To overcome all of these issues, we enlarged the simulation box for the *m*-crystal in the lateral dimensions from 4.5 × 5.3 to 9.0 × 10.5 nm. For similar reasons, the solvent phase is also enlarged in the *z* direction (compared with water), giving a final *z* dimension for the simulation box of 20.6 nm. The total number of *p*-nitroaniline molecules in the *m*-crystal case is 2304 with 5086 octanol molecules, and the total number of atoms in the system is just short of 174 000. In the case of the *c*-crystal, the total simulation box measures 9.3 × 8.9 × 20.6 nm containing 3072 *p*-nitroaniline and 3751 octanol molecules (~150 000 atoms).

RESULTS

The first indication that structuring of the solvent near the crystal surface occurs can be seen in the particle density plots perpendicular to the surface; see Figure 2. Both water and octanol exhibit strong structuring in multiple layers. For water this structuring fades after ~1.2 nm distance from the surface, but for octanol, it remains much longer, at least up to 2.8 nm. As a consequence, the hydration layers are also thicker in the case of octanol (see table next to Figure 2), going from on average 0.29 nm for water to 0.44 nm for octanol.

Comparison of the *m*-crystal and *c*-crystal for both solvents shows the density profiles being much flatter for the *c*-crystal (especially for the water case), although the differences disappear further away from the surface. The most plausible explanation for these more lowered densities is the nature of the exposed surface. For the *m*-crystal, this is a rather homogeneous structure, whereas the surface for the *c*-crystal exhibits much more heterogeneity; see Figure 1d.

To compare our MD results directly with the AFM experiments, we computed the 2-D density profiles parallel to the surface for each of the hydration layers. Because in general

localization of water is strongest in the first hydration layer, we focus our studies of the water density in this regime as a first approximation of what the AFM experiments are likely to see. Furthermore, we assume the local densities to be directly related to the forces the AFM feels, leading to the topography image. This is a simplification, and more elaborate methods exist, such as modeling the tip as a nanocluster[21] or converting local densities through Boltzmann inversion into free-energy curves,[22] but in the end it is the local density (if left largely undisturbed by the tip) that determines the AFM image. So at least a qualitative comparison is possible.

In Figure 3, both of the results (topography and cross-sectional Δf distributions, a, b, e, and f) from the previously performed experiments,[14] as well as the 2D particle density plots (c and g) and snapshots (d and h) from the MD simulation with water as a solvent are shown. In the experiments, two different topographies have been observed, one with two spots of equal brightness in the unit cell (observed only in limited cases, named 'rare' in this paper) and one with a bright and a less bright spot in each unit cell (named 'common' here). For the common cases, also cross-sectional Δf distributions (perpendicular to the (101) plane and along either the [101] or [010] direction) have been measured in the experiments. In the topography images, Figures 3a,e, the unit cell is indicated by the dashed line, and in the Δf distribution of the [101] direction, Figure 3b, the solid yellow arrows indicate the observed major grooves, which are 1.5 nm apart.

The snapshots shown in Figure 3d,h are visually time-combined, which means that each atom for each snapshot (one each 0.5 ps) is drawn into the image, with the more recent ones drawn on top of the others. As such, these images provide an accumulated view on where atoms have been over time. However, it does not tell us how long an atom remains at the given position. The particle density distributions shown in Figure 3c,g take this residence time into account. It must be noted that to compute the 2D particle density distributions only the oxygen atoms of the water molecules have been taken into account. For the *m*-crystal, higher densities are visible at several spots, and most of them lie on virtual vertical lines. This coincides very well with the observed hydrogen atom locations in the corresponding snapshot. (These visible hydrogen atoms are closer to the surface than their corresponding oxygen
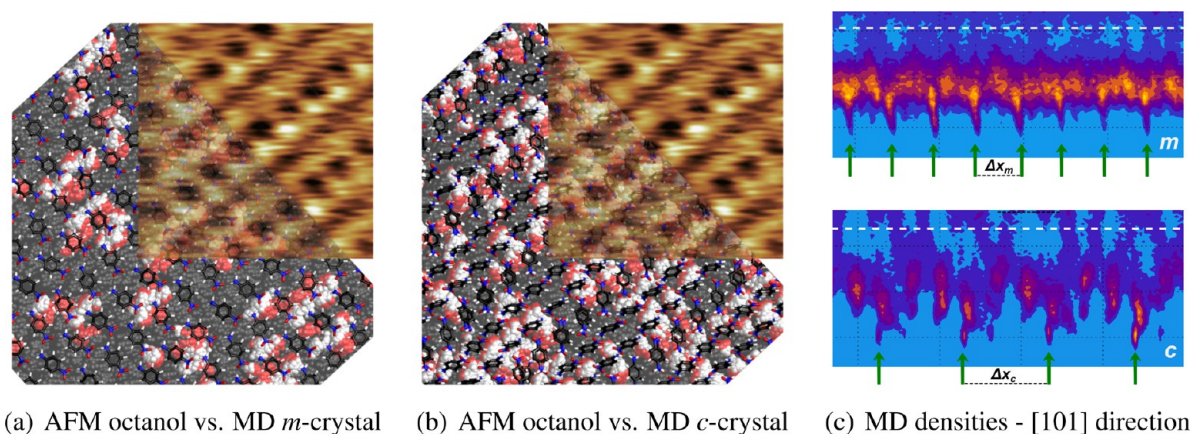
(a) AFM octanol vs. MD *m*-crystal   (b) AFM octanol vs. MD *c*-crystal   (c) MD densities - [101] direction

Figure 5. Composite images comparing the AFM octanol topography images to both the MD snapshots for the *m*-crystal (a) and the *c*-crystal (b). In panel c, the cross-sectional density plots along the [101] direction as obtained from the MD simulations are shown, with the periodicity indicated by the green arrows.

atoms, but in the snapshot image they block the view to the oxygen atoms; these oxygen atoms are, however, located in the same hydration layer as all the visible oxygen atoms, and thus, in the density plots next to the snapshot images, these oxygens show up.) The distance between each of these lines of higher density spots is ~0.75 nm. In the case of the *c*-crystal, the particle density plot looks quite different. Some structural arrangements (high density, bright spots) are observed as well as crescent-shaped densities. The latter ones are located on top of the phenylene part of the *p*-nitroaniline molecules lying parallel to the (101) plane. Again, the bright spots align very well with the hydrogens observed in the snapshot image. One can observe two 'vertical' lines of bright spots, followed by a vertical line of crescent densities, which show, in combination with the snapshot, the higher densities to occur near the amino and nitro groups of the upright molecules in the *c*-crystal.

To enhance the comparison between experiments and simulations, we aligned our obtained images with the experimental ones. In Figure 4a,b, these composite images are shown for the top views (topography images and MD snapshots). In Figure 4a, the AFM topographic image from the rare cases shows excellent agreement with the MD snapshot, as obtained from the *m*-crystal simulations. Similarly, the AFM common case (see Figure 4b) is in strong agreement with the results from the *c*-crystal simulations; even the brighter and less bright spots can be identified to stem from the different hydrogen rows. In both cases, the darker spots in the experimental images agree very well with the location of the phenylenes.

In Figure 4c,d, the side views for the common case (the Δf distributions for both directions) are compared with the cross-sectional simulation density plots for both crystal types (m to the left, and c to the right). The green arrows indicate similar features appearing in each image (either experimental or from the simulations), with the corresponding spacing indicated by Δx or Δy, respectively. From the experiments, the values for these spacings were measured to be $\Delta x_{exp} = 1.5$ nm and $\Delta y_{exp} = 0.6$ nm. On the basis of the comparison between experiment and simulations, it is clear that $\Delta x_{exp} \approx \Delta x_c \approx 2 \cdot \Delta x_m$ and $\Delta y_{exp} \approx \Delta y_c \approx 2 \cdot \Delta y_m$, showing again the striking resemblance between the *c*-crystal and the AFM common case observations.

A similar AFM-MD comparison is done for the octanol case; see Figure 5. This time, there is neither a rare nor a common experimental observation, and the same AFM topographic

image is compared with both crystal arrangements. As with the results for water, the *c*-crystal has the better agreement. Also, the periodicity for the *c*-crystal, as observed along the [101] direction (see Figure 5c), is in better agreement with the experimental results, and, again, the periodicity for the *c*-crystal is twice the periodicity of the *m*-crystal.

It is interesting to emphasize this double periodicity within one unit cell observed in the *m*-crystal, which occurs only in the rare cases of the AFM experiments, but in the majority of the experiments, the periodicity is in line with the size of the unit cell. When the *m*-crystal would be the preferred exposed surface, one expects to see a double periodicity, simply based on symmetry arguments of the surface structure. However, for the *c*-crystal, such a symmetry argument is unnecessary, and one would expect the simple periodicity all the time. In our previous paper,[14] we explained brighter and fewer bright spots (the simple periodicity) as being caused by an alternate appearance of the modulated water density and especially along the [101] direction with every other nitro-group of *p*-nitroaniline having a stronger or less strong ordering interaction with the water. On the basis of our current simulation results, it seems more likely that the experimental surface is no longer of the *m*-crystal type but restructured to resemble the *c*-crystal. Only in rare cases is a double periodicity observed in the experiments, coinciding with the *m*-crystal.

In the previous crystallographic research on *p*-nitroaniline, no reconstruction of the free surface from the *m*-crystal to the *c*-crystal has been reported. To establish whether it is theoretically possible for a bulk *m*-crystal with a *c*-crystal surface to remain stable, we conducted additional MD simulations of surfaces exposed to the vacuum (free surface) of a large *m*-crystal with either no, one, or more *c*-crystal layers on top of the bulk *m*-crystal. For each layer in either the *m* or the *c* phase of the crystal, we computed the average potential energy per molecule within that layer. Obviously, molecules in either exposed layer have the highest potential energy, as they have neighboring molecules on only one side. In Figure 6, these energies per layer and per extra layer of the *c*-crystal are depicted. Without any *c*-crystal layer present, the energies are perfectly symmetrical (red line), but after the addition of one *c*-crystal layer the energy of the free *c* surface is slightly lower than that for the *m* surface, whereas the *m* layer next to the *c* has a higher energy compared with the bulk phase but a significantly lower energy than an *m* layer exposed to vacuum
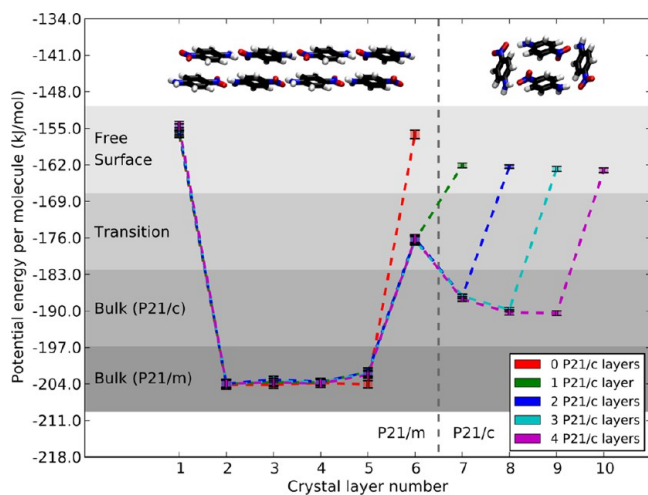
Figure 6. Potential energy per molecule in each layer of a combined *m*-crystal and *c* crystal *p*-nitroaniline structure. The different curves show the effects of none, one, or more *c*-crystal layers on top of a bulk *m*-crystal structure. The outer layers are exposed to vacuum, hence the free layers. The molecular arrangement is shown on top. (See also Figure 1d.)

(green line). Increasing the number of *c* layers, it appears that after three layers the *c*-crystal part reaches equilibrium and maintains its potential energy for the bulk phase for those parts not exposed to vacuum. Only at the interface can a potential energy penalty be observed, but it is not prohibitively large and could be overcome by a more favorable hydration energy at the surface. In all cases, the combined crystal structures are observed to be extremely stable.

For both crystal arrangements and solvents, we also computed this hydration energy (per functional group of a *p*-nitroaniline molecule). In Figure 7a, these energies are shown for the cases with water as a solvent. The results for octanol are not shown here, as they are identical (except for the actual energy values, which are about half in the case of octanol). For the *m*-crystal, the hydration energy is quite homogeneously distributed along the surface with a slight hydrophilic favoring of the nitro groups and a modest hydrophobic interaction with the phenylene groups. In the case of the *c*-crystal, the picture is different, as the interaction with the phenylene group parallel to the surface is now neutral, and it is the exposed nitro group of the perpendicularly oriented *p*-nitroaniline molecule that has a
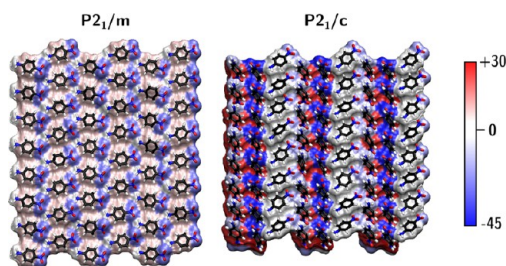
strong hydrophilic interaction. The stronger hydrophobic interaction is with the phenylene groups of the perpendicular molecule, but these are buried deeper inside the surface and as such have less interaction with the water.

Both of the previously mentioned arguments (stable combination and hydration energy) point toward the possibility of surface reconstruction. The only question remains as to how such a reconstruction could happen. One possible scenario is that after cleavage of the crystal the exposed surface restructures, either because of increased stress and strain in the crystal or because of debris from the cleavage being adsorbed and recrystallizing at the surface again but in a different crystal arrangement. It is also possible that in the AFM experiments the presence of the probe induces a surface reconstruction.
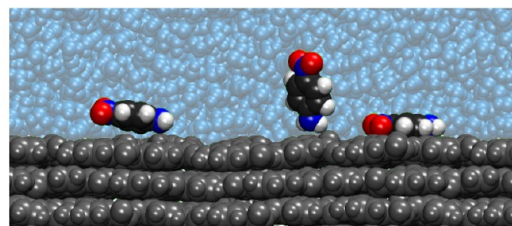
Of these scenarios, we have preliminary investigated the possibilities (using MD simulations) for the spontaneous adsorption of *p*-nitroaniline molecules onto a *m*-crystal. In Figure 7b, a snapshot from a stable situation in these simulations (where the concentration of free *p*-nitroaniline molecules is kept quite low as not to disturb the solid–liquid interface structure too much) is shown, where two *p*-nitroaniline molecules can be seen to be parallel to the surface but one molecule is perpendicularly oriented. Thus, it seems possible for a crystal to grow into a *c*-crystal, when *p*-nitroaniline molecules can stably adsorb perpendicular onto the surface. Unfortunately, current computational resources do not allow us to simulate the entire adsorption process, but we believe to have observed the preliminary stages of it.

■ DISCUSSION

In this work, we have combined experimental AFM measurements of the *p*-nitroaniline−water and *p*-nitroaniline−octanol interface with detailed MD simulations. By extensively using two possible surface arrangements (the *m*-crystal and *c*-crystal), we are able to match the results from the AFM water experiments almost exactly with the results from the MD simulations. Although in some situations the *m*-crystal appears in the AFM experiments, the *c*-crystal surface structure is much more commonly observed. In the case of octanol as a solvent, it is again shown that the *c*-crystal is the most likely surface structure. Additional computation showed that the existence of a few *c*-crystal layers on top of the *m*-crystal is possible, and some preliminary adsorption simulations show that this structure can form spontaneously as well.

(a) Local surface hydration energies (a.u.)

(b) Adsorbing *p*-nitroaniline on the *m*-crystal

Figure 7. In panel a, the local surface hydration energies at the exposed *p*-nitroaniline surface are shown as a color map with the actual molecular arrangement shown as well. On the left, the *m*-crystal is shown, and on the right, the *c*-crystal is shown. Blue encoded energies mean hydrophilic interaction and red encoded energies mean hydrophobic. In panel b, a snapshot from MD simulations of a *m*-crystal shows the adsorption of free *p*-nitroaniline molecules in solution onto the surface, in either parallel or perpendicular orientation.

Currently, this different surface structure has not been directly observed in crystallography (or any other non-AFM) experiments, as these were mainly focused on the bulk phase instead. As such, our findings on a possible reconstruction are quite new and open experimental challenges for it to be confirmed. In the past, surface reconstruction of inorganic crystals has been revealed with electron-based diffraction method (like LEED and RHEED),[39,40] as different crystal symmetries give rise to different diffraction patterns. However, organic compounds (like p-nitroaniline) are quite sensitive to electron irradiation, which makes direct observation challenging. Even more, the p-nitroaniline molecules in the m-crystal are alternatingly tilted to the surface plane with a small angle (<20°), which could give rise to a diffraction pattern similar to the one to be observed in the case of a c-crystal surface. Probably surface X-ray diffraction studies in either vacuum or water can be helpful to support our novel proposal of surface reconstruction in organic crystals like p-nitroaniline.

Our study emphasizes the power of high-resolution techniques to probe the solid–liquid interface in 3D, while demonstrating the importance of including systematic simulation approaches to confirm the details of the molecular structure. The work we presented in this paper shows the complexity of the solid–liquid interaction that occurs on the nanoscale, with the strong coupling between hydration layers and underlying molecular topography making interpretation far from straightforward. We also showed that it is possible to use both experimental and computational techniques to shed light on the effects of an heterogeneous surface, where the interactions with the solvent are dominated by the functional groups occurring on the surface of the crystal, which is an important step in better understanding the nature of complex solid–liquid interfaces.

So far we have looked only at flat surfaces, but for many applications, defects occurring at the surface prove to be important as nucleation point for recrystallization or chemical reactions.[41] Also, in these cases, it is important to understand the solvation structure at the surface and the effect solvated molecules within the hydration layers next to the crystal surface have. The solvation structure controls the desolvation process on the molecular scale, and understanding it is a critical step in the development of new applications, especially with respect to new medicines.[42] Applying our combined simulation and experimental approach to these more complex systems will be a key stage in the development of this field in the future.

■ AUTHOR INFORMATION

Corresponding Author
*E-mail: peter.spijker@aalto.fi. Phone: +358-50-4332614.

Notes
The authors declare no competing financial interest.

■ ACKNOWLEDGMENTS

■ REFERENCES

(1) Hugelmann, M.; Hugelmann, P.; Lorentz, W.; Schindler, W. Nanoelectrochemistry and Nanophysics at Electrochemical Interfaces. *Surf. Sci.* **2005**, *597*, 157−172.

(2) Whitesides, G. M.; Grzybowski, B. Self-Assembly at All Scales. *Science* **2002**, *295*, 2418−2421.

(3) Frauenfelder, H.; Fenimore, P. W.; Chen, G.; McMahon, B. H. Protein Folding is Slave to Solvent Motions. *Proc. Natl. Acad. Sci. U.S.A.* **2006**, *103*, 15469−15472.

(4) Fenter, P.; Sturchio, N. C. Mineral-Water Interfacial Structures Revealed by Synchrotron X-ray Scattering. *Prog. Surf. Sci.* **2004**, *77*, 171−258.

(5) Quate, C. F. The AFM as a Tool for Surface Imaging. *Surf. Sci.* **1994**, *299−300*, 980−995.

(6) Giessibl, F. J. Advances in Atomic Force Microscopy. *Rev. Mod. Phys.* **2003**, *75*, 949−983.

(7) Barth, C.; Foster, A. S.; Henry, C. R.; Shluger, A. L. Recent Trends in Surface Characterization and Chemistry with High-Resolution Scanning Force Methods. *Adv. Mater.* **2011**, *23*, 477−501.

(8) Voïtchovsky, K.; Kuna, J. J.; Contera, S. A.; Tosatti, E.; Stellacci, F. Direct Mapping of the Solid-Liquid Adhesion Energy with Subnanometre Resolution. *Nat. Nanotechnol.* **2010**, *5*, 401−405.

(9) Fukuma, T.; Ueda, Y.; Yoshioka, S.; Asakawa, H. Atomic-Scale Distribution of Water Molecules at the Mica-Water Interface Visualized by Three-Dimensional Scanning Force Microscopy. *Phys. Rev. Lett.* **2010**, *104*, 016101.

(10) O'Shea, S. J.; Lantz, M. A.; Tokumoto, H. Damping Near Solid-Liquid Interfaces Measured with Atomic Force Microscopy. *Langmuir* **1999**, *15*, 922−925.

(11) Hiasa, T.; Kimura, K.; Onishi, H. Hydration of Hydrophilic Thiolate Monolayers Visualized by Atomic Force Microscopy. *Phys. Chem. Chem. Phys.* **2012**, *14*, 8419−8424.

(12) Ricci, M.; Spijker, P.; Molinari, J. F.; Stellacci, F.; Voïtchovsky, K. Direct Visualization of Single Adsorbed Ions at the Surface of Calcite in Aqueous Environment. *Langmuir* **2013**, *29*, 2207−2216.

(13) Kobayashi, K.; Oyabu, N.; Kimura, K.; Ido, S.; Suzuki, K.; Imai, T.; Tagami, K.; Tsukada, M.; Yamada, H. Visualization of Hydration Layers on Muscovite Mica in Aqueous Solution by Frequency-Modulation Atomic Force Microscopy. *J. Chem. Phys.* **2013**, *138*, 184704.

(14) Nishioka, R.; Hiasa, T.; Kimura, K.; Onishi, H. AFM Study of Specific Hydration on p-Nitroaniline Crystal. *J. Phys. Chem. C* **2013**, *117*, 2939−2943.

(15) Ward, M. D. Bulk Crystals to Surfaces: Combining X-ray Diffraction and Atomic Force Microscopy to Probe the Structure and Formation of Crystal Interfaces. *Chem. Rev.* **2001**, *101*, 1697−1725.

(16) Abrahams, S. C.; Monteath Robertson, J. The Crystal Structure of p-Nitroaniline, NO₂.C₆H₄.NH₂. *Acta Crystallogr.* **1948**, *1*, 252−259.

(17) Donohue, J.; Trueblood, K. N. The Crystal Structure of p-Nitroaniline. *Acta Crystallogr.* **1956**, *9*, 960−965.

(18) Trueblood, K. N.; Goldish, E.; Donohue, J. A Three-Dimensional Refinement of the Crystal Structure of 4-Nitroaniline. *Acta Crystallogr.* **1961**, *14*, 1009−1017.

(19) Etter, M. C. Hydrogen Bonds as Design Elements in Organic Chemistry. *J. Phys. Chem.* **1991**, *95*, 4601−4610.

(20) Kobayahsi, H.; Kotani, M. Study of Single Crystal Surface with Second-Harmonic Generation: p-Nitroaniline. *Mol. Cryst. Liq. Cryst.* **1994**, *252*, 277−281.

(21) Reischl, B.; Watkins, M.; Foster, A. S. Free Energy Approaches for Modeling Atomic Force Microscopy in Liquids. *J. Chem. Theory Comput.* **2013**, *9*, 600−608.

(22) Watkins, M.; Reischl, B. A Simple Approximation for Forces Exerted on an AFM Tip in Liquid. *J. Chem. Phys.* **2013**, *138*, 154703.

(23) Brooks, B. R.; Brooks, C. L.; Mackerell, A. D.; Nilsson, L.; Petrella, R. J.; Roux, B.; Won, Y.; Archontis, G.; Bartels, C.; Boresch, S.; et al. CHARMM: The Biomolecular Simulation Program. *J. Comput. Chem.* **2009**, *30*, 1545−1614.

(24) Coombes, D. S.; Price, S. L.; Willock, D. J.; Leslie, M. Role of Electrostatic Interactions in Determining the Crystal Structures of Polar Organic Molecules. A Distributed Multipole Study. *J. Phys. Chem.* **1996**, *100*, 7352−7360.

(25) Kresse, G.; Furthmüller, J. Efficiency of Ab-Initio Total Energy Calculations for Metals and Semiconductors Using a Plane-Wave Basis Set. *Comput. Mater. Sci.* **1996**, *6*, 15−50.

(26) Kresse, G.; Furthmüller, J. Efficient Iterative Schemes for Ab Initio Total-Energy Calculations Using a Plane-Wave Basis Set. *Phys. Rev. B* **1996**, *54*, 11169.

(27) Perdew, J. P.; Burke, K.; Ernzerhof, M. Generalized Gradient Approximation Made Simple. *Phys. Rev. Lett.* **1996**, *77*, 3865–3868.

(28) Lee, K.; Murray, É.; Kong, L.; Lundqvist, B.; Langreth, D. Higher-Accuracy Van Der Waals Density Functional. *Phys. Rev. B* **2010**, *82*, 081101.

(29) Gulans, A.; Puska, M. J.; Nieminen, R. M. Linear-Scaling Self-Consistent Implementation of the Van Der Waals Density Functional. *Phys. Rev. B* **2009**, *79*, 201105.

(30) Blöchl, P. E. Projector Augmented-Wave Method. *Phys. Rev. B* **1994**, *50*, 17953–17979.

(31) Kresse, G.; Joubert, D. From Ultrasoft Pseudopotentials to the Projector Augmented-Wave Method. *Phys. Rev. B* **1999**, *59*, 1758–1775.

(32) Henkelman, G.; Arnaldsson, A.; Jónson, H. A Fast and Robust Algorithm for Bader Decomposition of Charge Density. *Comput. Mater. Sci.* **2006**, *36*, 354–360.

(33) Phillips, J. C.; Braun, R.; Wang, W.; Gumbart, J.; Tajkhorshid, E.; Villa, E.; Chipot, C.; Skeel, R. D.; Kale, L.; Schulten, K. Scalable Molecular Dynamics with NAMD. *J. Comput. Chem.* **2005**, *26*, 1781–1802.

(34) Helttunen, K.; Lehtovaara, L.; Häkkinen, H.; Nissinen, M. Crystal Structures and Density Functional Theory Calculations of o- and p-Nitroaniline Derivatives: Combined Effect of Hydrogen Bonding and Aromatic Interactions on Dimerization Energy. *Cryst. Growth Des.* **2013**, *13*, 3603–3612.

(35) Humphrey, W.; Dalke, A.; Schulten, K. VMD - Visual Molecular Dynamics. *J. Mol. Graphics* **1996**, *14*, 33–38.

(36) Michaud-Agrawal, N.; Denning, E. J.; Woolf, T. B.; Beckstein, O. MDAnalysis: A Toolkit for the Analysis of Molecular Dynamics Simulations. *J. Comput. Chem.* **2011**, *32*, 2319–2327.

(37) Watkins, M.; Shluger, A. L. Mechanism of Contrast Formation in Atomic Force Microscopy in Water. *Phys. Rev. Let.* **2010**, *105*, 196101.

(38) Pecharsky, V.; Zavalij, P. *Fundamentals of Powder Diffraction and Structural Characterization of Materials*; Springer: New York, 2005.

(39) Liang, Y.; Gan, S.; Chambers, S.; Altman, E. Surface Structure of Anatase TiO2(001): Reconstruction, Atomic Steps, and Domains. *Phys. Rev. B* **2001**, *63*, 235402.

(40) Seki, K.; Hayashi, N.; Oji, H.; Ito, E.; Ouchi, Y.; Ishii, H. Electronic Structure of Organic/Metal Interfaces. *Thin Solid Films* **2001**, *393*, 298–303.

(41) Raiteri, P.; Gale, J. D.; Quigley, D.; Rodger, P. M. Derivation of an Accurate Force-Field for Simulating the Growth of Calcium Carbonate from Aqueous Solution: A New Model for the Calcite-Water Interface. *J. Phys. Chem. C* **2010**, *114*, 5997–6010.

(42) Somasundaran, P.; Huang, L. Adsorption/Aggregation of Surfactants and Their Mixtures at Solid-Liquid Interfaces. *Adv. Colloid Interface Sci.* **2000**, *88*, 179–208.